# Diffuse Mid-UV Communication in the Presence of Obscurants

Derek P. Young, Jerry Brewer, Jeannette Chang, Tina Chou, Jacques Kvam and Matthew Pugh
Sandia National Laboratories
Livermore, California

***Abstract*—Communication using mid-ultraviolet radiation between 200 nm and 280 nm has received renewed attention due to advancements in UV LED emitters and unique propagation characteristics at these wavelengths. Atmospheric gases absorb light at mid-UV so that receivers or sensors operating on the earth's surface receive no interference from solar radiation. This so-called "solar-blind" region of the spectrum allows the use of single-photon detection techniques. Further, UV light is strongly scattered by molecules in the air, enabling non-line-of-sight (NLOS) communication. We extend previous work in this area by incorporating angle-dependent Mie scattering into one of the standard propagation models, in an effort to include the effects of aerosols. Experimental results from outdoor measurements using a fog generator are also presented.**

## I. Introduction

Wireless communication using diffuse mid-UV is enabled by two unique phenomena: the atmosphere absorbs solar radiation between 200 nm and 280 nm, and UV generated on the earth's surface is strongly scattered [1]–[3]. Because mid-UV radiation from the sun is absorbed by the atmosphere, receivers on the ground operate in a nearly noise-free environment. In conjunction, the strong scattering enables non-line-of-sight (NLOS) communication. NLOS UV communication systems are well-suited for link distances on the order of 10–100 m in applications such as unattended ground sensor networks.

An analytical non-line-of-sight (NLOS) single-scatter model for UV propagation has been published by Luettgen, Shapiro, and Reilly [4]. This model integrates scattered light from the intersection of two cones (representing the transmitter divergence and the receiver field-of-view) assuming that any light reaching the receiver sensor scattered only one time. Luettgen's single-scatter model is a standard in recent research. However, some researchers have noted that the single-scatter model underestimates the delay spread and received power when compared to experimental measurements and Monte Carlo simulation [5]. Still, the analytical model provides reasonable and convenient results.

Real-world applications require that we better understand the operation of the NLOS UV link under non-ideal conditions—fog or smoke may obscure part of the communication link. This paper describes work done to quantify these effects. The following sections discuss modifications made to Luettgen's model to support analysis with obscurants and preliminary measurements made outdoors using a fog generator.

Sandia National Laboratories is a multi-program laboratory managed and operated by Sandia Corporation, a wholly owned subsidiary of Lockheed Martin Corporation, for the U.S. Department of Energy's National Nuclear Security Administration under contract DE-AC04-94AL85000. SAND No. 2012-9972C

## II. Modeling

The propagation of UV light can be described in terms of scattering and absorption. For molecular scattering, Rayleigh's theory can be used effectively, but for particle diameters approaching the wavelength of incident light, scattering becomes much more complicated, and Mie scattering is more applicable [6].

We used Luettgen's model in our work to consider system trade-offs involved in designing a UV communication link. We modified the model to include the effects of Mie scattering in order to analyze the effects of obscurants such as fog and smoke. The presence of additional particles in the path of the emitted UV light adds additional attenuation, but it also introduces additional sources of scattering that can redirect light toward the receiver in a NLOS configuration.

### A. Single Scatter Model

The model developed by Luettgen, et al. calculates the impulse response for optical radiation in a homogeneous scattering and absorbing medium [4]. Properties of the medium are incorporated using scattering and absorption coefficients. Setup of the calculation is straight-forward. However, calculating the intersection of the transmit and receive cones requires the use of a prolate-spheroidal coordinate system. Figures and results from [4] are repeated here for convenience because we use the same notation when making modifications. Interested readers should refer to the original paper for details of the derivation.

The single-scatter model based on the prolate-spheroidal coordinate system is illustrated in Fig. 1. This coordinate system is convenient because the sum of the distances from the foci to any point on the spheroid surface is constant (for a given $\xi$). In the single scatter model, this physically means that each value of $\xi$ corresponds to a particular time delay in the impulse response. This relationship is given by (1), where $c$ is the speed of light, $t$ is time, and $r$ is the distance between transmitter and receiver.

$$\xi = \frac{ct}{r} \tag{1}$$

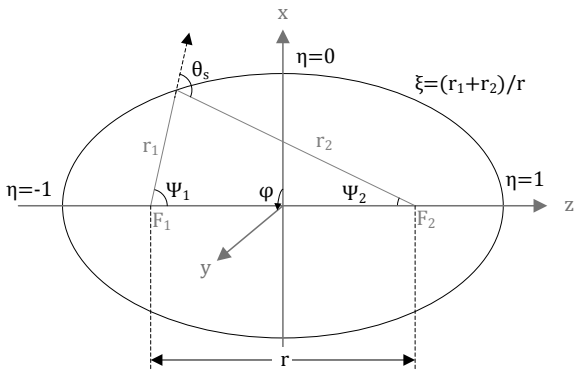


Fig. 1. Prolate-spheroid coordinate system

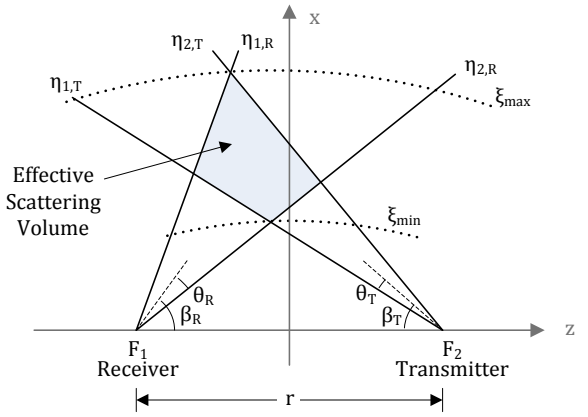


Fig. 2. Non-line-of-sight geometry for single-scatter propagation model

Fig. 2 shows an example NLOS geometry with parameters labeled. The single-scatter model uses the following parameters:

| | |
|---|---|
| $\theta_R$ | Receiver half-field of view $(0 \leq \theta_R \leq \pi/2)$ [rad] |
| $\beta_R$ | Receiver apex angle $(0 \leq \beta_R \leq \pi)$ [rad] |
| $\theta_T$ | Transmitter beam divergence half angle $(0 \leq \theta_T \leq \pi/2)$ [rad] |
| $\beta_T$ | Transmitter apex angle $(0 \leq \beta_T \leq \pi)$ [rad] |
| $Q_T$ | Energy of an impulse transmitted at time $t = 0$ [J] |
| $k_s$ | Atmospheric scatter coefficient [$m^{-1}$] |
| $k_a$ | Atmospheric absorption coefficient [$m^{-1}$] |
| $k_e$ | Atmospheric extinction coefficient [$m^{-1}$] |
| $\Omega_T$ | Transmitter solid cone angle [sr] |
| $P(\theta_s)$ | Normalized scattering phase function |
| $r$ | Interfocal distance [m] |

The extinction coefficient is the sum of the scatter and absorption coefficients as shown in (2).

$$k_e = k_s + k_a \tag{2}$$

To solve for the impulse response of the channel, first consider an impulse of energy $Q_T$ emitted at time $t = 0$ from the transmitter. The unextinguished energy per unit area at a point $P$ within the transmitter cone is then derived. The differential volume containing this point effectively becomes a new source. The contributions from all such sources within the intersection of the transmit and receive cones are integrated to produce the impulse response of the channel. Equation (3) gives irradiance ($W/m^2$) as a function of time when $\xi$ is between $\xi_{min}$ and $\xi_{max}$. $E(\xi)$ is zero outside this range.

$$E(\xi) = \frac{Q_t c k_s \exp(-k_e r \xi)}{2\pi\Omega_T r^2} \int_{\eta_1(\xi)}^{\eta_2(\xi)} \frac{2g[\phi_2(\xi,\eta)]P(\theta_s)}{\xi^2 - \eta^2}\, \mathrm{d}\eta \tag{3}$$

The values $\xi_{min}$ and $\xi_{max}$ correspond to the minimum and maximum time for which scattered energy is received for a transmitted impulse. The limits of integration, $\eta_1(\xi)$ and $\eta_2(\xi)$, and the function $g[\phi_2(\xi,\eta)]$ depend on the geometry of the optics. Please refer to [4] for detailed derivation and description of these values.

Numerical integration of (3) was performed using MATLAB's built-in adaptive Gauss-Kronrod quadrature algorithm, `quadgk`.

### *B. Single Scatter Model with Obscurants*

In order to model the effects of obscurants such as fog and smoke, Mie scattering must be taken into account because the aerosol particle diameters are comparable to mid-UV wavelengths [6]. Under the single-scatter assumption, effects from the scattering and absorption caused by obscurants can simply be added to the scattering and absorption due to molecular scattering characterized by Rayleigh's equations. Obscurant particles add both additional attenuation as well as additional scattering. Previous papers have modeled Mie scattering through the use of a weighting function [7]. We instead used a published computer code to directly compute the phase function [8].

To accommodate the possibility of mixed obscurants with different density, particle diameters, and composition, we introduce a discretized population of particle diameters, $D_i$. For each value of $D_i$, there is an associated concentration, $C_i$, and an associated complex refractive index, $M_i$. From these, we calculate extinction, scattering and absorption coefficients ($k_{em,i}$, $k_{sm,i}$ and $k_{am,i}$) using the Mie code for each index $i$. The subscript $_m$ has been appended to distinguish the new Mie coefficients from the Rayleigh coefficients. The particle size distribution is discrete for simplicity, but the number of bins can be made arbitrarily large if greater resolution is required.

The equations from [4] can now be modified to accommodate the added particulates. Additional attenuation is included to account for added particles in the propagation path. Equation (4) shows the unextinguished energy per unit area at the scattering point, $P$, after adding this attenuation. In this section, all modified equations are marked with a $'$ symbol.

$$H'_P = \frac{Q_T}{\Omega_T (r_2)^2} \left[ \mathrm{e}^{-k_e r_2} \mathrm{e}^{-k_{em,1} r_2} \mathrm{e}^{-k_{em,2} r_2} \ldots \right] = \frac{Q_T}{\Omega_T (r_2)^2} e^{-K_e r_2} \quad (4)$$

Rayleigh and Mie coefficients are combined into a total extinction coefficient, $K_e$.

$$K_e = k_e + \sum_i k_{em,i} \quad (5)$$

The energy scattered from location $P$ becomes

$$\delta Q'_P = k_s H'_P \delta V + \sum_i k_{sm,i} H'_P \delta V. \quad (6)$$

Applying the Rayleigh phase function, $P_r(\theta_s)$, and Mie phase functions, $P_{m,i}(\theta_s)$, to the appropriate terms, the energy transmitted from $P$ per unit solid angle is then

$$\delta R'_P = \left[ k_s H'_P \frac{P_r(\theta_s)}{4\pi} + \sum_i k_{sm,i} H'_P \frac{P_{m,i}(\theta_s)}{4\pi} \right] \delta V. \quad (7)$$

Note that for each particle index, $i$, there is a different scattering coefficient, $k_{sm,i}$, and phase function, $P_{m,i}(\theta_s)$. The energy from all these contributions are summed for a particular scattering angle, $\theta_s$.

At the receiver, the energy per unit area in prolate-spheroid coordinates is

$$\delta H'_R = \delta R'_P \frac{\cos(\zeta) \exp(-K_e r_1)}{(r_1)^2}. \quad (8)$$

The irradiance at the receiver sourced by a differential volume on the spheroid specified by $\xi$, is then given by

$$\delta E'(\xi) = \frac{Q_T c k_s \cos(\zeta) \exp(-K_e r \xi)}{2\pi \Omega_T r^2 (\xi^2 - \eta^2)} P_r(\theta_s)\, \delta\phi \delta\eta + \sum_i \frac{Q_T c k_{sm,i} \cos(\zeta) \exp(-K_e r \xi)}{2\pi \Omega_T r^2 (\xi^2 - \eta^2)} P_{m,i}(\theta_s)\, \delta\phi \delta\eta. \quad (9)$$

Integrating as before and switching the order of summation and integration gives the received irradiance, $E'(\xi)$, for values of $\xi$ between $\xi_{min}$ and $\xi_{max}$. (Again, $E'(\xi)$ is zero outside this range.) The limits of integration remain unchanged from the original model.

$$E'(\xi) = \frac{Q_t c k_s \exp(-K_e r \xi)}{2\pi \Omega_T r^2} \int_{\eta_1(\xi)}^{\eta_2(\xi)} \frac{2g[\phi_2(\xi,\eta)] P_r(\theta_s)}{\xi^2 - \eta^2} \mathrm{d}\eta + \sum_i \left[ \frac{Q_t c k_{sm,i} \exp(-K_e r \xi)}{2\pi \Omega_T r^2} \int_{\eta_1(\xi)}^{\eta_2(\xi)} \frac{2g[\phi_2(\xi,\eta)] P_{m,i}(\theta_s)}{\xi^2 - \eta^2} \mathrm{d}\eta \right] \quad (10)$$

Given the array of particles sizes and their characteristics, coefficients are calculated using the Mie code. The total extinction coefficient is computed by summing all the extinction coefficients. The irradiance is then computed for each particle type separately (the phase function is specified uniquely by the particle size parameter and the index of refraction), and the result is summed.

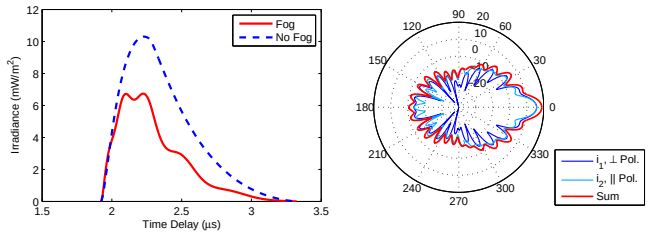


(a) (b)

Fig. 3. (a) Example impulse response comparing clear atmosphere versus fog. (b) Mie phase function for particles of $m = 1.33$ and $\alpha = 12.6$. Amplitude expressed in dB.

Fig. 3 shows example results assuming a 1 J impulse at 250 nm. In the model, the receiver and transmitter were placed 500 m apart. The transmit and receive cone half angles were $\pi/12$, and the elevation angles were $\pi/4$. The plot compares results for clear atmosphere versus a uniform fog of 1 µm water droplets (which have an index of refraction of $m = 1.33$ and a size parameter of $\alpha = 12.6$), with a density of $10^9$ particles/m$^3$. The Mie phase function was computed using [8]. This example includes only a single particle type, but the computer code allows the modeling of an arbitrary distribution of particles.

## III. Measurements

Outdoor tests were performed using commercial LED emitters from Sensor Electronic Technology, operating at 267±5 nm. For the receiver, we used a Perkin Elmer C1922 channel photo multiplier (CPM) fitted with an optical filter from Ofil Technologies. The filter has a nominal passband of 260–276 nm. The optical density is greater than 8 in the stop band. Aerosols were introduced into the optical channel by using a portable Vi-Count 1300 fog generator, manufactured by Corona Integrated Technologies (nominal particle size 0.2–0.3 µm).

A sequence of 20 recordings was made for each combination of range, receiver elevation angle, and presence or absence of fog. Each sequence required four minutes to record. During each measurement, the transmitter continuously transmitted a pseudo-random sequence of bits. Fog was released for 30 seconds at the maximum flow rate at the start of some measurement sequences. Separate measurements were also made to establish dark count and solar count baselines. The CPM output was directly recorded using a high-speed oscilloscope and the data was post-processed in MATLAB. A diagram of the system configuration is shown in Fig. 5, photographs of hardware components are shown in Fig. 4, and test parameters are summarized in Table I.

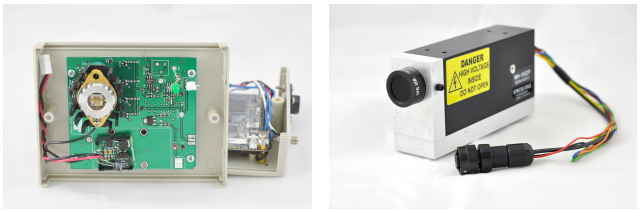

(a) (b)

Fig. 4. Hardware for outdoor testing: (a) Transmitter module showing commercial LED array, (b) Channel photo multiplier with mounted 268 nm filter

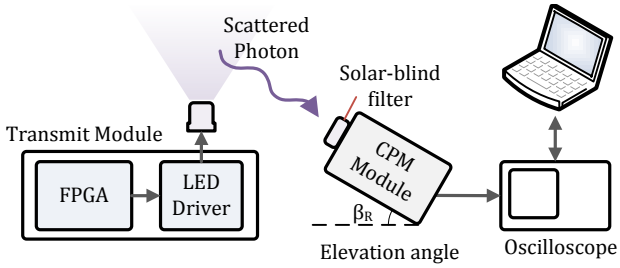


Fig. 5. Diagram of measurement system

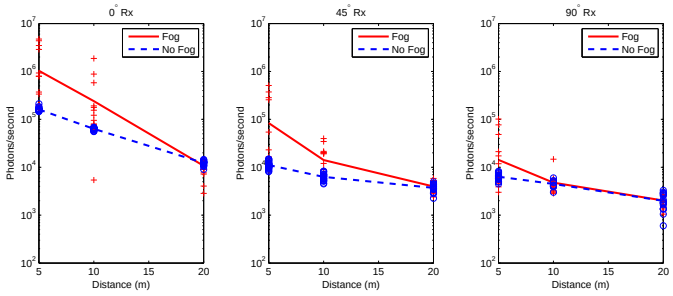


Fig. 6. Results of experiment showing effect of fog on communication link for three different receiver elevation angles: 0°, 45°, 90°

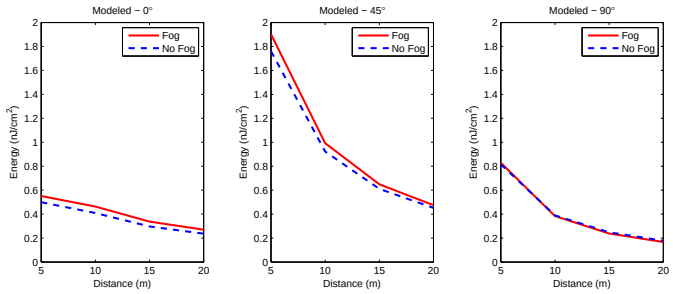


Fig. 7. Modeled response, assuming parameters used in the experiment setup and fog density of $10^{10}$ particles/m$^3$

## IV. Results and Conclusions

The number of photons received for various receiver elevation angles and separation distances are shown in Fig. 6. Measured results show that more photons were received in the presence of fog. This is supported by our model, which predicts that for many of the geometries and parameters we tested, more photons are received with the addition of fog. Fig. 7 shows the modeled response for our test parameters and an assumed fog density. We expect some discrepancy because the model assumes uniform density fog, while in practice, the fog was non-uniform. The number of measured photons is much lower than predicted by the model, but the number of photons received is comparable to the numbers reported by other researchers [1].

For short ranges, the benefits of additional scattering due to the fog outweigh the detriment of the added attenuation. At longer distances, however, we expect that the extra attenuation would dominate. The measurements reported in this paper represent preliminary work. Future work would improve upon the calibration techniques and better control the test environment.

TABLE I
Test System Parameters

| **Transmit parameters** | |
|---|---|
| LED peak wavelength | 267 nm |
| Divergence | ±40° |
| Elevation angle | 90° (zenith) |
| Optical power | 15 mW |
| Modulation | 2 PPM |
| Duty cycle | 33% |
| Pulse width | 5 µs |
| **Receive parameters** | |
| Optical filter insertion loss | 8 dB |
| Field of view | 60° |
| Test range | 5, 10, 20 m |
| Elevation angle | 0°, 45°, 90° |
| Receive duration | 20 ms |


## Acknowledgment

Thanks to our collaborators Mary Crawford and Andy Allerman. Also, special thanks to Tom Reichardt and Steven Paradise.


## References


[1] G. A. Shaw, A. M. Siegel, J. Model, and D. Greisokh, "Recent progress in short-range ultraviolet communication," *SPIE*, vol. 5796, pp. 214–225, 2005.

[2] Z. Xu and B. M. Sadler, "Ultraviolet communications: Potential and state-of-the-art," *IEEE Commun. Mag.*, 2008.

[3] D. M. Reilly, D. T. Moriarty, and J. A. Maynard, "Unique properties of solar blind ultraviolet communication systems for unattended ground sensor networks," *SPIE*, vol. 5611, pp. 244–254, 2005.

[4] M. R. Luettgen, J. H. Shapiro, and D. M. Reilly, "Non-line-of-sight single-scatter propagation model," *Journal of the Optical Societ of America*, pp. 1964–1972, 1991.

[5] H. Ding, G. Chen, A. K. Majumdar, B. M. Sadler, and Z. Xu, "Modeling of non-line-of-sight ultraviolet scattering channels for communication," *IEEE J. Sel. Areas Commun.*, 2009.

[6] W. C. Hinds, *Aerosol Technology*, 2nd ed. John Wiley and Sons, 1999.

[7] Z. Xu, H. Ding, B. M. Sadler, and G. Chen, "Analytical performance study of solar blind non-line-of-sight ultraviolet short-range communication links," *Optics Letters*, pp. 1860–1862, 2008.

[8] C. Matzler. (2002) Matlab functions for mie scattering and absorption. Code: http://diogenes.iwt.uni-bremen.de/vt/laser/codes/Mie-Matlab-Maetzler.zip. [Online]. Available: http://arrc.ou.edu/~rockee/NRA_2007_website/Mie-scattering-Matlab.pdf